Accepted Manuscript

Mechanical coupling of microtubule-dependent motor teams during peroxisome transport in Drosophila S2 cells

María Cecilia De Rossi, Diana E. Wetzler, Lorena Benseñor, María Emilia De Rossi, Mariela Sued, Daniela Rodríguez, Vladimir Gelfand, Luciana Bruno, Valeria Levi

Please cite this article as: María Cecilia De Rossi, Diana E. Wetzler, Lorena Benseñor, María Emilia De Rossi, Mariela Sued, Daniela Rodríguez, Vladimir Gelfand, Luciana Bruno, Valeria Levi , Mechanical coupling of microtubule-dependent motor teams during peroxisome transport in Drosophila S2 cells, (2017), doi: 10.1016/j.bbagen.2017.09.009

Mechanical coupling of microtubule-dependent motor teams during peroxisome transport in *Drosophila* S2 cells

María Cecilia De Rossi [a,b], Diana E. Wetzler [a,b], Lorena Benseñor [c], María Emilia De Rossi [d,e], Mariela Sued [f], Daniela Rodríguez [f], Vladimir Gelfand [g], Luciana Bruno [h,i*] and Valeria Levi [a,b*]

[a]Universidad de Buenos Aires. Facultad de Ciencias Exactas y Naturales. Departamento de Química Biológica, Laboratorio de Dinámica Intracelular. Buenos Aires, Argentina.
[b]CONICET- Universidad de Buenos Aires. Instituto de Química Biológica de la Facultad de Ciencias Exactas y Naturales (IQUIBICEN). Buenos Aires, Argentina.
[c]Fundación Instituto Leloir. CONICET. Buenos Aires, Argentina.
[d]Universidad de Buenos Aires, Facultad de Ciencias Exactas y Naturales y Ciclo Básico Común. Buenos Aires, Argentina
[e]CONICET- Universidad de Buenos Aires, Instituto de Astronomía y Física del Espacio (IAFE). Buenos Aires, Argentina.
[f]Universidad de Buenos Aires. Facultad de Ciencias Exactas y Naturales. Instituto de Cálculo. Buenos Aires, Argentina.
[g]Department of Cell and Molecular Biology, Feinberg School of Medicine, Northwestern University, Chicago, IL 60611, USA.
[h]Universidad de Buenos Aires. Facultad de Ciencias Exactas y Naturales. Departamento de Física. Buenos Aires, Argentina.
[i]CONICET- Universidad de Buenos Aires. Instituto de Física de Buenos Aires (IFIBA). Buenos Aires, Argentina.

[*]To whom correspondence should be addressed. E-mails: vlevi12@gmail.com and lbruno@df.uba.ar. Phone and fax: 0054-114-786-3426.

Abstract

Background: Intracellular transport requires molecular motors that step along cytoskeletal filaments actively dragging cargoes through the crowded cytoplasm. Here, we explore the interplay of the opposed polarity motors kinesin-1 and cytoplasmic dynein during peroxisome transport along microtubules in *Drosophila* S2 cells.

Methods: We used single particle tracking with nanometer accuracy and millisecond time resolution to extract quantitative information on the bidirectional motion of organelles. The transport performance was studied in cells expressing a slow chimeric plus-end directed motor or the kinesin heavy chain. We also analyzed the influence of peroxisomes membrane fluidity in methyl-β-ciclodextrin treated cells. The experimental data was also confronted with numerical simulations of two well-established tug of war scenarios.

Results and conclusions: The velocity distributions of retrograde and anterograde peroxisomes showed a multimodal pattern suggesting that multiple motor teams drive transport in either direction. The chimeric motors interfered with the performance of anterograde transport and also reduced the speed of the slowest retrograde team. In addition, increasing the fluidity of peroxisomes membrane decreased the speed of the slowest anterograde and retrograde teams.

General Significance: Our results support the existence of a crosstalk between opposed-polarity motor teams. Moreover, the slowest teams seem to mechanically communicate with each other through the membrane to trigger transport.

Keywords

Abbreviations

SPT, single particle tracking; KHC, kinesin heavy chain; MβCD, methyl-β-cyclodextrin; GP, generalized polarization.

1. Introduction

Transport of vesicles, organelles and other cellular cargoes is central to a wide variety of biological processes (reviewed in [1-3]). Intracellular transport relies on molecular motors that step along cytoskeletal filaments actively dragging cargoes through the crowded cytoplasm. Several neurodegenerative diseases such as Alzheimer's, Huntington's and Parkinson's involve failures on intracellular transport mechanisms [4-9] emphasizing the relevance of understanding the rules of this active process. The biophysical properties of motor proteins have been extensively studied with single-molecule techniques (e.g. [10-13]) however these studies could not completely reveal how transport develops in living cells.

Cargoes attach simultaneously dynein and kinesin motors which move toward the minus and plus end of microtubules and define bidirectional trajectories with frequent switches in direction [2]. Theoretical and experimental studies proposed that opposed polarity motors compete with each other, those motors exerting more force win the tug of war and determine the cargo direction (e.g. [10, 14-16]). Transport mechanisms *in vivo* seem to be far more complex since the selective motor recruitment to specific cargoes [17] and their interactions with several regulatory proteins (reviewed in [18]) may also bias the natural tug of war and contribute to define the organelle directionality. In some transport processes regulatory mechanisms prevail and cargoes present a sustained unidirectional motion whereas tug of war is predominant in others leading to a more erratic, saltatory motion (reviewed in [19]).

In this work, we explore how microtubule motors work together during peroxisome transport in *Drosophila* S2 cells. These cells present large and rigid microtubule processes after depolymerization of the actin network and thus they constitute an ideal system for studies of microtubule motors *in vivo*. Kinesin-1 and cytoplasmic dynein (hereafter referred to as dynein) drive peroxisome transport in this system [20-22];

In a previous work, Ally et al. [20] depleted S2 cells of either the plus-end or the minus-end directed motors and replaced them with exogenous motors. They focused their analysis on exploring peroxisomes distribution in the cells (e.g. whether they are in the perinuclear region or the tips or shafts of the processes) and counted the number of "vectors" defined as "*the distance moved by a single peroxisome in 1 s*" above a threshold value of 0.2 μm. Based on their observation, they proposed that these motors require each other for sustained motion in either direction.

We now used this well-established cellular system to obtain mechanistic insights on the coordination and competition among microtubule motors. With this aim, we employed single particle tracking (SPT) with nanometer accuracy and millisecond time resolution; these high temporal and spatial resolutions allow capturing hidden details of bidirectional motion. We assessed the robustness of retrograde and anterograde teams and included in the system a slow plus-end directed motor that competes with the endogenous motors. We also confronted these experimental data with the predictions obtained from numerical simulations of tug of war scenarios. Finally, we modified the

3

organelles membrane fluidity to test the mechanical coupling among opposed motor teams.

Our results demonstrate that peroxisome transport cannot be explained by simple tug of war models and suggest that slow anterograde and retrograde teams mechanically comunicate with each other through the organelle membrane. This comunication seems necessary to establish the rapid motion of peroxisomes along microtubules.

2. Materials and methods

2.1 Cell culture and transfections

Drosophila melanogaster S2 cells were cultured as described in [23]. Cells were grown in Schneider´s Media (Sigma-Aldrich) supplemented with 10% FBS. SPT experiments were performed using a stable cell line expressing the peroxisomes signal peptide SKL fused to EGFP [20].

The influence of exogenous motors on transport was studied in S2 cells expressing either the dimeric version of *Xenopus* Eg5 (amino acids 1-513, referred as Eg5(513), [20]) or the kinesin 1 heavy chain (amino acids 1-576, named as KHC576, [24]). The cargo and autoinhibitory domains of the protein are removed in this truncated, KHC576 motor resulting in a constitutively active version of kinesin-1 [25-27].

Motors were cloned into $CuSO_4$ inducible plasmids encoding the human peroxin family protein Pex26 (amino acids 245-305) fused to mCherry (mCherry-Pex26) as an artificial N-terminal motor tag to direct the motors onto peroxisomes [20].

Eg5(513)-mCherry-Pex26 was transiently transfected in a S2 cell line stably expressing the peroxisome signal peptide SKL-EGFP. The experiments involving KHC576 were performed in a S2 cell line stably expressing both the SKL-EGFP and KHC576-mCherry-Pex26 [20].

Transfections were performed using Effectene (QIAGEN) following the vendor instructions. The motors expression was induced adding to the medium 0.4 mM CuSO4 (final concentration) 24 hs before imaging.

2.2 Cells preparation for imaging experiments

For microscopy measurements, 25-mm round coverslips previously modified with 500 µg/ml of concanavalin A (Sigma-Aldrich) were mounted in a custom-made chamber specially designed for the microscope. Cells were added to the chamber and incubated in 0.5 ml of serum-free medium containing 10 mM of latrunculin B (Sigma-Aldrich) for 15 min to promote actin depolimerization.

2.3 Cholesterol depletion and membrane fluidity analysis

Cholesterol depletion from cell membranes was induced incubating the cells with 10 mM of methyl-β-cyclodextrin (MβCD) for 15 min [28].

Membrane fluidity was assessed incubating the cells with 50 nM C-Laurdan during 5 min [28]. This probe senses the polarity of its microenvironment through a spectral shift

of its emission and informs on the local fluidity since loosely packed membranes present a higher penetration of water molecules.

2.4 Confocal microscopy

Confocal images were acquired in FV1000 Olympus confocal microscopes (Olympus Inc, Japan). EGFP and mCherry fusion proteins were observed using a multi-line Ar laser tuned at 488 nm and a solid diode laser of 543 nm as excitation source, respectively. The laser light was reflected by a dichroic mirror (DM 405/488/543/635) and focused through an Olympus UPlanSApo 60x oil immersion objective (NA = 1.35) onto the sample. Fluorescence was collected by the same objective and split into two channels set to collect photons in the range 500–525 nm (EGFP) and 650-750 nm (mCherry). Fluorescence was detected with photomultipliers set in the photon-counting detection mode.

C-Laurdan images were collected using a solid diode laser at 405 nm. The laser light was reflected by a dichroic mirror (DM 405/488/543/635) and focused through an Olympus UPlanSApo 60X water immersion objective (NA= 1.20) onto the sample. Fluorescence of C-laurdan was collected into two independent detectors set to simultaneously collect fluorescence in the range 430- 470 nm and 505-525 nm (channels 1 and 2, respectively).

2.5 Generalized polarization (GP) imaging

GP images were obtained from these images computing the apparent GP at every pixel as follows (Eq. 1):

$$GP_{app} = \frac{I_{430-470} - G \cdot I_{505-525}}{I_{430-470} + G \cdot I_{505-525}} \quad (1)$$

where $I_{430-470}$ and $I_{505-525}$ correspond to the fluorescence intensity collected in channels 1 and 2, respectively. The G factor was determined using a solution 10 µM C-laurdan in DMSO following a procedure similar to that described previously [29].
GP analysis was performed using the ImageJ software.

2.6 Tracking experiments

SPT experiments were carried out in a Nikon Eclipse TE300 fluorescence microscope adapted for SPT using a 60X oil-immersion objective (NA: 1.35). A high-speed electron-multiplying CCD camera (DVC 340 M, Thorlabs Inc) was coupled to the video port of the microscope for imaging the cells. We recorded movies (2000 frames) of individual fluorescent peroxisomes at a speed of 100 frames/s. The organelles trajectories were recovered with an accuracy in the range of 3-5 nm using the pattern recognition tracking algorithm previously described in [30].
Briefly, the program sets the initial coordinates of the peroxisome and generates an intensity pattern that consists of the average intensity obtained from the first 10 frames of a region containing the organelle image. This pattern is stored in the computer

memory to be used during the calculation of the peroxisome position through the image stack.

To calculate the peroxisome position in the next frame, the algorithm compares the intensity distributions of the pattern with that of five areas of the frame that have the same size as the pattern, the first area is centered at the pattern and the others are shifted $\pm$ n pixels in the x (horizontal) or y (vertical) directions. In the experiments presented in this work, n = 2, however, this number can be adjusted by the operator.

For each of these areas, the weighted deviation (δ) is calculated as follows (Eq. 2):

$$\delta = \sum_{i,j} \sqrt{(I_{imagej}(i,j) - I_{pattern}(i,j) - B)^2} \times w(i,j) \, (2)$$

where $I(i,j)$ is the intensity at position (i,j), B is the difference between the average backgrounds of the local image and the pattern, and $w(i,j)$ is a weighting factor that attributes more weight to points with higher contrast.

The values of δ obtained for the areas in the x and y directions are interpolated with parabolic functions. From the interpolations, a minimum value of δ can be determined in the x and y directions. Then, the center area is repositioned to the new coordinates and the minimization routine is repeated as explained until the particle position is determined with a given tolerance, typically 1/100 of a pixel. Since the minimum of the parabolas can be located at fractional values of a pixel, the intensity of the image needs to be interpolated at the overlapping positions; this operation is done with a bilinear interpolation.

The number of analyzed trajectories in each experimental condition was 200-300, obtained from ~200 cells.

2.7 Trajectories analysis

Peroxisomes trajectories were split and classified according to the direction of movement into plus (toward the tip of a process) and minus (toward the cell center) directed motion. These curvilinear sections of the trajectories were fitted with second order polynomial functions to compute the traveled distance as a function of time; those sections that present clear beginning and end positions were considered as a run and included in the run length statistics. We restricted the analyses to regions of the trajectories where the organelles traveled at speeds > 0.1 μm/s for at least 0.45 μm.

The determination of the organelle speeds from the trajectories requires the evaluation of the distance traveled by the organelle in a time interval; since the velocity is not constant along the trajectories the speed values always depend on the evaluated time window. The "arbitrary" selection of time intervals for speed determinations is widely used in the organelle- transport literature (see for example [9, 23, 35]). In this work, segmental speeds were obtained by splitting the sections of directed motion into segments of 40 points, each segment was fitted with a linear equation; the slope, that corresponds to the velocity, was computed in the segmental velocity statistics when the chi-squared value is higher than 0.9 or discarded otherwise. This constraint restricts the analysis to trajectory segments where peroxisomes are moving at approximately constant speed. We selected a 400 ms- time window since shorter intervals introduce

high-speed artifacts due to thermal jittering and longer intervals may include short reversions on the direction that result in lower speed values.

The number of plus and minus segments analyzed in each experimental condition ranged 1500-2700.

The trajectories analysis was performed using algorithms programmed in IDL (Interactive Data Language).

2.8 Numerical simulation

We used a tug of war model [14, 31, 32] similar to that described previously [33, 34] with the parameters described in Supplemental Table 1. In this scenario, the cargo is driven by opposed-polarity motors (i.e. kinesins and dyneins), which act as parallel springs with elastic constant κ_0. The motors move stochastically in discrete 8-nm steps along an unidimensional track, with load-dependent probabilities of stepping and detachment. Detached motors can rebind the track with a constant probability. The biophysical parameter of Eg5(513) motors were similar to those of kinesin with the exception of the velocity at zero load, which was considered 10-fold lower than that of kinesin [35].

Cooperation among dynein motors in the asymmetric model was included as a stepwise increment of the attachment probability dependent on the number of motors already bound to the microtubule.

After each simulation step, we computed the number of kinesin and dynein motors attached to the track which were further defined as active motors. These configurations do not change significantly within 10-ms time window (Supplemental Fig. 1) and thus, we speeded up the analysis assigning the motor configuration determined at the end of each 10 ms time interval as representative of the whole interval.

The simulated trajectories (time step = 10 μs) were resampled to 10 ms (i.e. the experimental sampling time) and analyzed following the procedures previously described for those obtained experimentally.

The simulation algorithm runs within a MATLAB environment and can be downloaded from the website http://www.gdti.df.uba.ar/

2.9 Statistical analysis.

The speed distribution was analyzed using a Gaussian mixture model [36] that considers the data as a combination of samples obtained from K normal distributions.

Since this method avoids fitting of histograms, it strength lies in the robustness of the determination of the parameters characterizing the underlying functions These mixture models allow making statistical inferences about the properties of the sub-populations given only observations on the pooled population. Moreover, the method does not require information regarding the sub-population identities.

Speed distributions analysis was performed assuming that K subpopulations are present, each of them distributed normally with mean v_k (k = 1,...,K). Similarly to a previous

work [30], we considered a common standard deviation (σ) since the experimental noise, the tracking error and most important, variations in the rheological properties of the organelle´s microenvironment are expected to spread out similarly every peak of the speed distributions. We should mention that other works (e.g. [9]) have also analyzed segmental speeds distributions using a multi-gaussian approach with different waists; both models provide empirical descriptions of the speed distributions and most important, allows detecting changes in the distribution when the transport system is perturbed.

The distribution f(v) is then represented as (Eq. 3):

$$f(v) = \sum_{k=1}^{K} p_k \frac{1}{\sqrt{2\pi}\sigma} e^{-\frac{1}{2}\left(\frac{v-v_k}{\sigma}\right)^2} \quad \textbf{(3)}$$

where p_k (k = 1,...,K) represents the relative size of the k-subpopulation with $\sum_{k=1}^{K} p_k = 1$

The center v_k of each subpopulation is a local maximum of the density distribution, and are named *modes* of the multimodal distribution.

The maximum likelihood estimators of the parameters (σ, v_k, p_k with k = 1,.., K) were obtained through the Expectation-Maximization algorithm previously described in [37] and the model was selected following the Bayesian information criterion (BIC, [36, 38]).

The parameters´ errors were computed by a bootstrap procedure, a widely used technique for estimating standard errors (SE) and confidence intervals, among other properties of the distribution of an estimator [39]. The method only assumes that the sample distribution is a good approximation to the population distribution, i.e. that the sample is representative of the population. Briefly, the bootstrap procedure generate M new data sets (i.e. bootstrap samples) by randomly sampling with replacement from the observed data to obtain new samples of the same size. The SE is then computed as indicated in Eq. 4. It can be demonstrated that the bootstrap method approximates the standard error of the estimator when the number of bootstrap samples M is large.

$$SE = \frac{1}{M} \sum_i \sqrt{(X_{med,i} - \overline{X_{med}})^2}) \quad \textbf{(4)}$$

where i is the data set number, M is the number of data sets and $\overline{X_{med}}$ the mean of $X_{med,i}$.

Run length median values were compared using the statistical test described in [34]. We used this parameter since it is more robust than the mean when the distribution of data is asymmetric [18]. The variance was estimated through the bootstrap procedure [39] described before.

In order to test whether the medians of different data groups are significantly different, we performed a hypothesis test with *p*-values obtained as follows (Eq. 5):

$$p\text{-value} = 2\left[1 - F\left(\frac{|\text{med}_{(g1)} - \text{med}_{(g2)}|}{\sqrt{\text{var}_{(g1)} + \text{var}_{(g2)}}}\right)\right] \textbf{(5)}$$

where F is the standard normal distribution and var(g1) and var(g2) represent the variance of each data group.

Statistical data analysis was performed using the R software.

Wilcoxon rank-sum test [40] was used to compare the distributions of apparent GP values obtained under control conditions and MβCD treatment.
The statistical analyses were performed using the software.

3. Results

3.1 A slow plus-end directed motor affects anterograde and retrograde transport of peroxisomes

We first explored the interplay between opposed-polarity microtubule motors during peroxisome transport in *Drosophila* S2 cells stably expressing the peroxisome targeting peptide SKL fused to EGFP [20]. With this aim, we treated the cells with latrunculin to depolymerize the actin network and recorded image stacks at 100 frames/s. The uniformly oriented bundles of microtubules, forming the core of processes generated by the cell in the absence of the actin network [23] simplify the assignation of the overall transport direction. Moreover, processes can be considered static in the time window of the experiments (Fig. 1A) as assessed by tracking the processes with a tracking routine that we have developed to track single filaments [41]. The algorithm shows the absence of significant motion of processes within the time window of the tracking experiments.
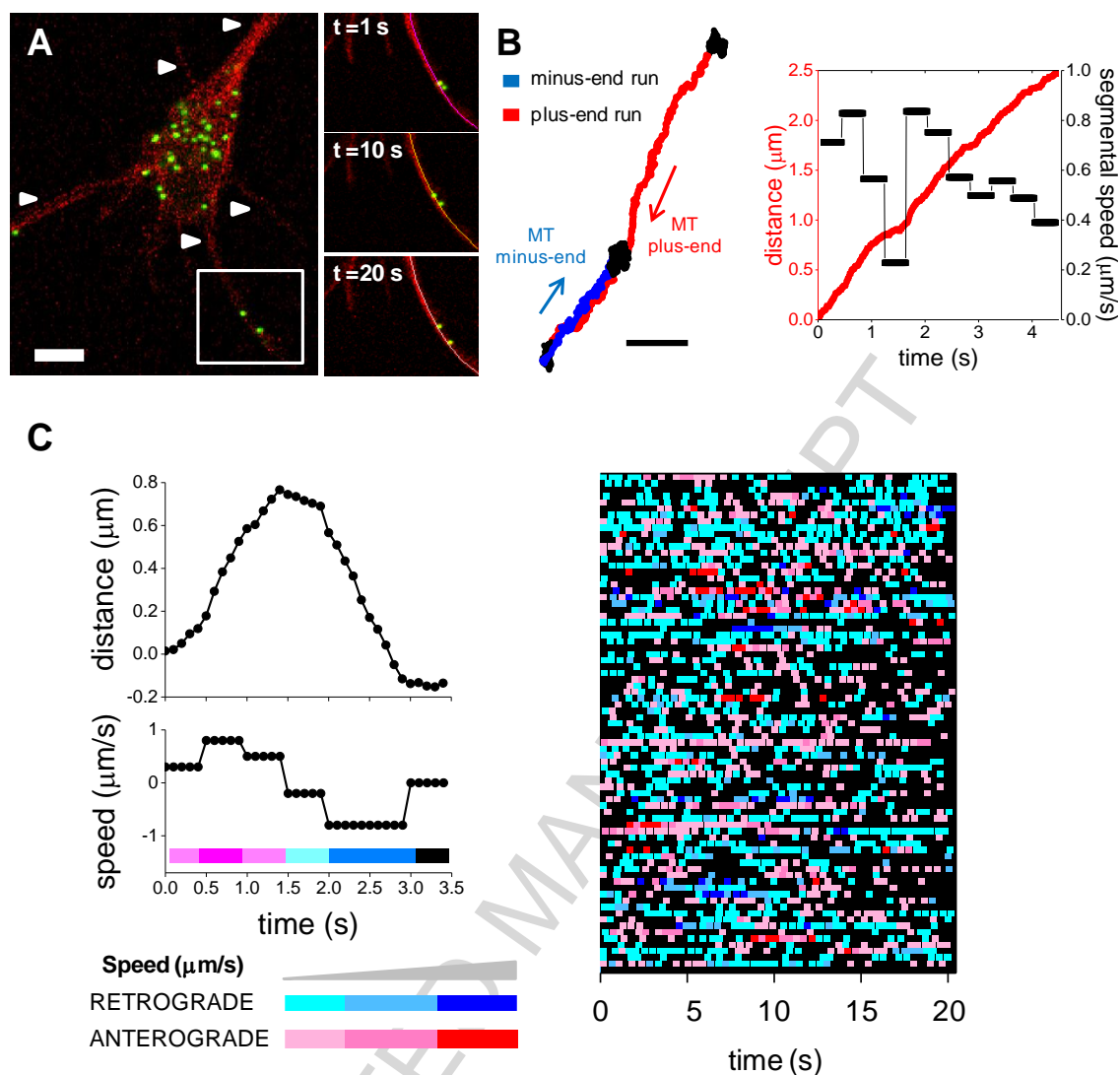
Fig. 1. **Trajectory analysis and temporal evolution of the peroxisomes speed.** Representative image of *D. melanogaster* S2 cell coexpressing mCherry-α-tubulin and the peroxisome signal peptide SKL-EGFP (**A**). The arrows indicate cellular processes. Scale bar: 5 μm. Image-stacks of a region (inset) were acquired as a function of time and the cellular process was tracked as a function of time with a filament-tracking routine. Representative trajectory obtained for a peroxisome (**B**). Trajectories were divided into unidirectional and uninterrupted paths (runs) corresponding to the motion towards the minus- (blue) or plus- (red) end of microtubule (MT). Scale bar: 0.5 μm. These runs were further analyzed as described in Materials and Methods to obtain the distance traveled as a function of time (red line) and the segmental speeds (●). The values of speeds were color-coded according to the organelle direction and relative speed values (0.1-0.7 μm/s, 0.7-1.0 μm/s and >1.0 μm/s) and represented as a function of time (**C**). The highest speed modes are shown in blue (retrograde) and red (anterograde). Those regions of the trajectories in which the speed could not be determined or it was lower than the threshold value (0.1 μm/s) were color-coded in

black. Each row of the matrix corresponds to a single trajectory ($N_{trajectories}$=78 from 67 cells). A cartoon illustrating the data analysis is shown in the left panel.

The relatively high data acquisition frequency allowed extracting detailed information regarding the local dynamics of organelles that can be missed when only considering low resolution or mean parameters [42]. These movies were analyzed with a pattern-recognition algorithm [30] to obtain peroxisome trajectories with a precision of 3-5 nm.

Peroxisome trajectories show periods of anterograde and retrograde transport interspersed with pauses or fluctuations in the transport direction (Fig. 1B). We split the trajectories into minus-end and plus-end directed runs and focused our analyses on two parameters, the segmental speed, proposed to be related to the configuration of motors that actively move the organelles [43, 44], and the run length, that informs on the mechanisms of deactivation of motor teams [42].

We qualitatively analyzed the temporal sequence of velocities in every trajectory and observed that fast and slow segments are interspersed in the trajectories (Fig. 1C) suggesting that there are not distinct populations of slow and fast organelles. This figure also shows a very low probability of reversions from a highest-speed retrograde to a highest-speed anterograde states (i.e. 4 of 42 reversions) and viceversa (2 of 47 reversions) suggesting that these fast states require the previous engagement of slower teams to switch the peroxisome direction of motion.

The multimodal velocity distributions of anterograde and retrograde organelles (Fig. 2A-B) suggest that multiple teams of motors are responsible for transport in either direction [43]. In contrast, simplified motor systems *in vitro* present single-peak distributions (e.g. [45, 46]). Therefore, the speed distribution provides a richer description than the analysis of the mean speed and could help us to reveal certain aspects of *in vivo* transport.

Anterograde and retrograde runs (Fig. 2, C-D and Table 1) presented characteristic median lengths of 991 ± 110 nm and 1064 ± 70 nm, respectively. These values are in the order of those measured for organelles and single motors moving in cells (e.g. [27]) and lower than those determined *in vitro* for teams of kinesin [47] and for dynein-dynactin-cargo adapter complexes [48] suggesting a different mechanism for the *in vivo* inactivation of motor teams.
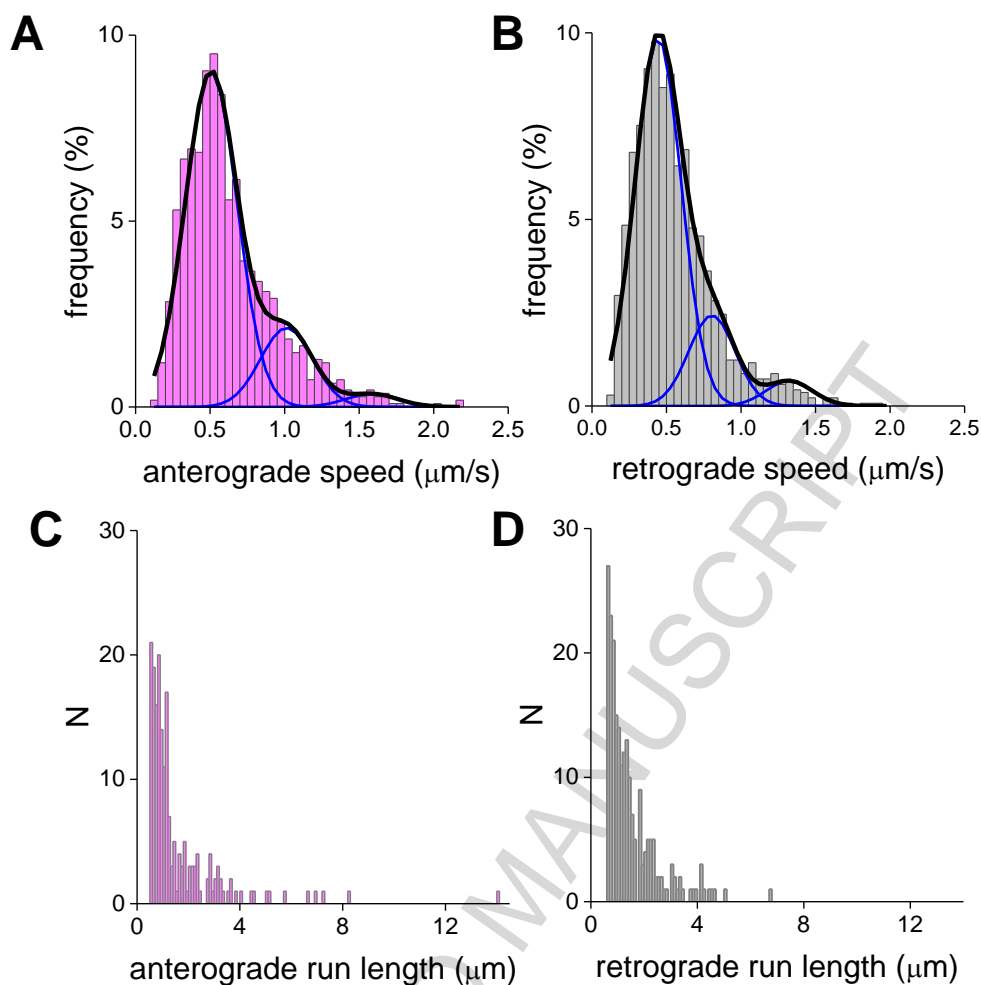
Fig. 2. Distributions of peroxisomes segmental speed and run length. Peroxisomes trajectories with nanometer precision were analyzed to recover the distribution of segmental speed **(A-B)** and run lengths **(C-D)** of anterograde and retrograde peroxisomes. The speed distributions were quantitatively analyzed as described in Section 2.9 considering a mixture of Gaussian functions (Eq. 3, black lines) with three modes (blue lines).

Next, we included in the cell system a deficient plus-end directed motor that competes with the endogenous cytoplasmic dynein and kinesin-1. Specifically, we used a construct that encodes the head, neck-linker, and first coiled-coil domains of the Eg5 motor fused to a peroxisome-signaling tag mCherry-Pex26 [20]. Eg5 is a heterotetrameric motor involved in microtubule motion during cell division [49, 50]; the dimeric version of the motor preserves many functional properties of the tetramer [35, 51]. Dimeric Eg5(513) is characterized by its low processivity (~ 70 nm) and speed (< 100 nm/s). Previous works also showed that the stall force of this motor [35, 52] and the kinetic constants of disociation from and association to microtubules [53-55] are similar to those of kinesin-1.

12

In a previous work, replacement of endogenous kinesin-1 by Eg5(513)-mCherry-Pex26 induced the clustering of peroxisomes in the perinuclear region [20]. In contrast, expression of this mutant in the wild type background showed peroxisomes in other cellular regions (Supplemental Fig. 2). The proportion of cell processes containing peroxisomes was identical to that determined in the wild type condition (~60 %) suggesting that the extra-motor does not drastically perturb the system.

Fig. 3A,C,G and Supplemental Table 2 show that Eg5(513)-mCherry-Pex26 significantly reduces the speed of anterograde peroxisomes with a redistribution of the populations toward the lowest-velocity mode (k=1); herein defined as the slowest population. The parsing algorithm used in our work considers that organelles are actively moving when their speed exceeds 100 nm/s. Since this threshold is similar to the *in vitro* speed of Eg5(513), we do not expect to detect pure Eg5(513)-mCherry-Pex26 teams dragging plus-end directed peroxisomes.

On the other hand, the speed distribution of retrograde organelles shows that the slowest population decreased by 18 % of its characteristic speed (Fig. 3D,F,H and Supplemental Table 3). In addition, Eg5(513)-mCherry-Pex 26 expression reduced the run lengths of both, anterograde and retrograde peroxisomes (Table 1). These observations show that anterograde motors also influence the retrograde teams performance.

The number of reversions per trajectory observed in the presence of Eg5(513) was not significantly different to that measured in the wild type condition (1.8 ± 0.1 vs. 1.80 ± 0.08) suggesting that the mutant motor introduces pauses and does not trigger switches in the transport direction.

3.2 KHC targeted to peroxisomes preserves many motility properties of the endogenous kinesin motor

To further explore whether the motor-organelle coupling strategy influences the performance of anterograde and retrograde teams we used the kinesin construct KHC576-mCherry-Pex26 [20] encoding amino acids 1–576 of *Drosophila* KHC fused to the mCherry-Pex26 linker used in the previous section. The overall organization of peroxisomes in the cytoplasm is conserved in the presence of the mutant since 60 % of processes presented organelles (Supplemental Fig. 2).

We run SPT experiments to follow the motion of SKL-EGFP labeled peroxisomes in S2 cells expressing KHC576-mCherry-Pex26 and computed the speed and run length distributions of anterograde and retrograde organelles. Fig. 3E,F,H and Supplemental Table 3 show that the multimode speed distribution of minus-end directed organelles is insensitive to the presence of Pex-targeted KHC576 motor whereas slow plus-end directed organelles reduce their speed (Figure 3B,C,G and Supplemental Table 2). This result is unexpected since the single-motor performance of the construct is similar or even better than that of the full-length motor according to *in vitro* and *in vivo* assays

[56, 57]. Thus, the artificial linker and/or truncation in KHC576-mCherry-Pex26 may affect the communication and thus the performance of anterograde teams which are probably constituted by at least two motor molecules. In line with this hypothesis, Bieling et al. [58] proposed that motors within kinesin teams mechanically communicate with each other and showed that a stiffer coupling reduces the cargo velocity.

On the other hand, the invariance of retrograde speeds distribution suggests that the endogenous and KHC576-mCherry-Pex26 motors contribute similarly to retrograde transport. In addition, KHC576-mCherry-Pex26 did not affect the median values of plus and minus-end directed run lengths (Table 1) and the number of reversions in the trajectories (1.8 ± 0.1 reversions/trajectory).

Overexpression of peroxisome-tagged KHC may introduce a higher concentration of plus-end directed motors in each organelle. In addition, truncation of kinesin molecule probably affects some of the regulatory mechanisms of the motor function e.g. those depending on KHC-KLC interactions [18]. Moreover, Pex26 linker prevents the detachment of KHC576 motors from the organelle. Thus, the invariance of run lengths with the expression of KHC576-mCherry-Pex (Table 1) suggests that retrograde and anterograde run terminations do not depend on these regulatory interactions or on kinesin attachment/detachment from the organelle.

In addition, a simple tug of war scenario predicts that a higher concentration of plus-end directed motors leads to more frequent switches from minus to plus-end directed runs resulting in a reduction of the lenghts of minus-end directed runs with a parallel increase of run lengths in the opposite direction ([15, 59], Supplemental Fig. 3). Thus, the invariance of anterograde and retrograde runs (Table 1) with the expression of KHC576-mCherry-Pex26 suggests that the number of plus-end directed motors involved in the active teams is similar to those observed in wild type cells. We hypothesize that the team size could be limited by geometrical constrains presented when motors attach simultaneously to the organelle and the microtubule [1] and/or by the interference among motors described for kinesin teams [60].
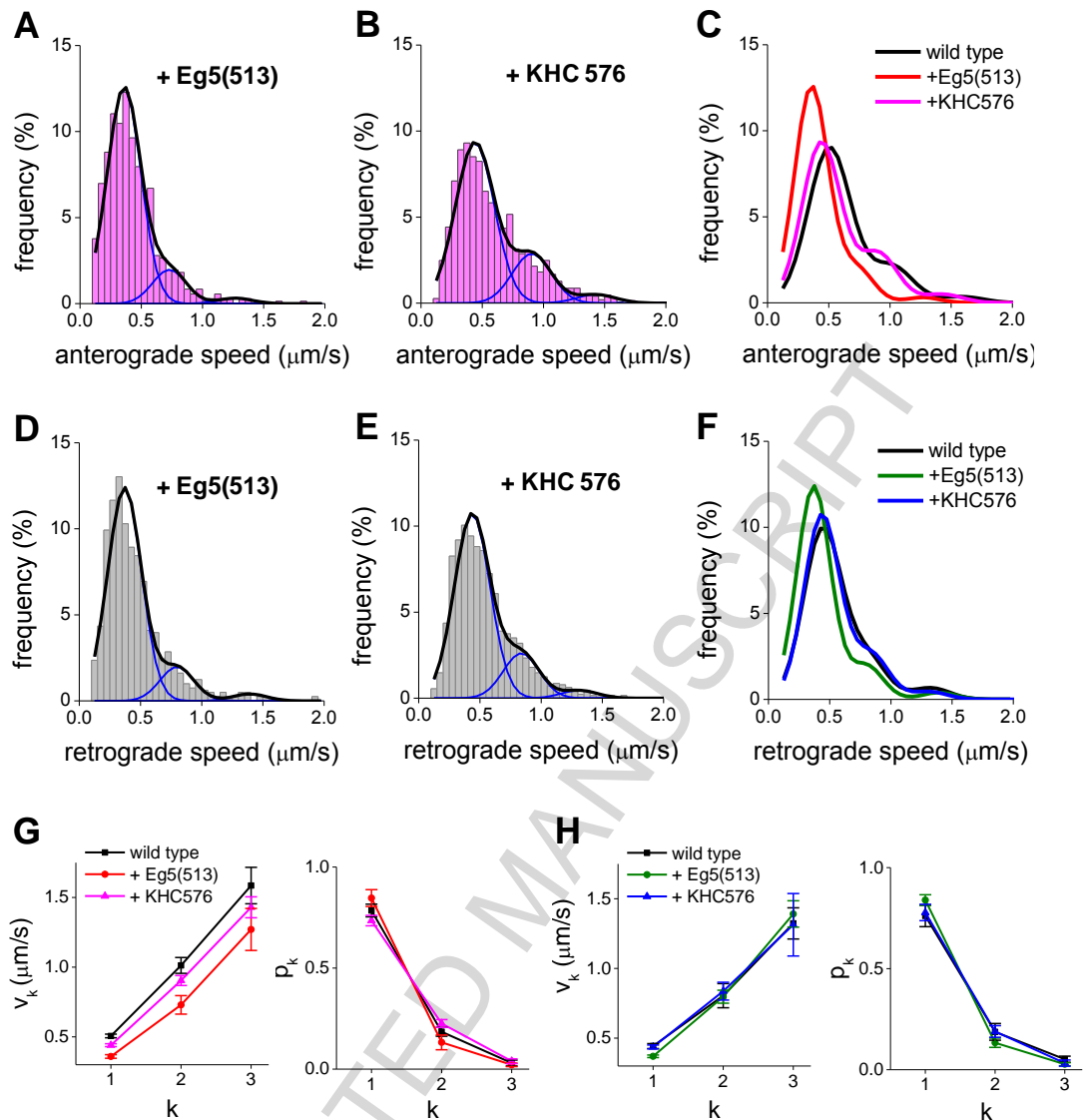
14

Fig. 3. Influence of Eg5(513) and KHC576 on peroxisomes transport. Single particle tracking experiments of EGFP-labeled peroxisomes were performed in cells expressing the deficient motility motor Eg5(513)-mCherry-Pex26 or the kinesin-1 like motor KHC576-mCherry-Pex26. Peroxisomes trajectories were further analyzed to obtain the distributions of anterograde **(A-C)** and retrograde **(D-F)** segmental speeds. These data were analyzed as described in Section 2.9 considering a mixture of 3 Gaussian functions (Eq. 3). Blue lines show the contributions of the individual Gaussians to the predicted overall distribution (black line). The mode speeds (v_k) and their relative contribution (p_k) to the overall distributions were compared with those obtained in the wild type condition **(G,H)** these parameters are also summarized in Supplemental Tables 2-3. The error bars represent standard errors of each parameter.

3.3 Tug of war scenarios do not completely explain peroxisome transport in S2 cells

To get further insights into the molecular mechanisms involved in peroxisome transport, we confronted the experimental data with numerical simulations of two established tug of war scenarios. Specifically, the asymmetric model considers the competition of multiple dyneins with a reduced number of kinesins [15, 61]. The teams' asymmetry accounts for the different biophysical properties of the motors including the higher stall force of kinesin-1 with respect to mammalian and *Dictyostelium* dyneins [12, 61, 62] and the different response of the motors to opposing forces [61]. On the other hand, we also studied the predictions of a symmetric tug of war model that takes into account recent findings showing that dynactin and Bicaudal-D2 increases the speed and stall force of dynein [10]. This strong dynein complex resists kinesin-1 during tug of war [10].

These tug of war models include 14-15 parameters, many of them estimated from *in vitro* experiments and thus the agreement of their predictions with the experimental data does not prove the validity of the models [1]. Therefore, we focused our analyses on an overall qualitative comparison of the main transport properties predicted from these models with those observed in S2 cells.

In the simulations, inactive motors move randomly on the surface of a cargo with a diffusion coefficient of 0.1 μm^2/s, i.e. in the order of those observed for membrane-associated proteins [63]. This consideration takes into account experimental and theoretical results showing that motor mobility within the membrane affect transport properties [64, 65]. Plus- and minus-end directed motors may stochastically attach to the microtubule, step along the track and detach from it. The parameters and equations characterizing these probabilities are comparable to those proposed in the literature (Supplemental Table 1, [15, 31, 34, 66-71]).

The simulated cargo trajectories were then resampled to 10 ms (i.e. the experimental sampling time) and analyzed similarly to the experimental data to recover the speed and run lengths distributions for cargoes moving in either direction. To better understand the output of the simulations, we also computed the number of motors attached to the track as described in Materials and Methods.

In order to set the total number of plus and minus-end directed motors in each scenario, we first run control simulations with increasing numbers of motors and selected the smallest values that generate trajectories compatible with those obtained experimentally.

Fig. 4, A-B and Supplemental Tables 4-5, show that a symmetric tug of war consisting of 4 kinesins competing with 4 strong dynein complexes qualitatively reproduced the multimode speed distributions of anterograde and retrograde peroxisomes. We described in Materials and Methods and also exemplified in Supplementary Fig. 1 that the simulation routine allows obtaining the motor configuration (i.e. the number of active dyneins and kinesin) at each sampling time. Then, we can correlate the motor

16

configurations and the segmental velocities measured at every 400-ms interval of the trajectories.

Fig. 4C shows that the speed distributions of the different motor configurations are partially overlapped. Teams with a high number of kinesin copies or highly enriched in dyneins contribute to the high-velocity modes. Low velocity anterograde and retrograde modes arise from configurations with low numbers of kinesins or mixed tug of war states with similar numbers of kinesin and dynein motors.

We also explored how a plus-end directed motor with the properties of Eg5(513) (Supplemental Table 1) modulates the symmetric tug of war. Importantly, we did not include in the model the back-stepping probability of this motor since it is expected to be low [35]. For these simulations, we assumed the number of motors in a plus-end directed team to be approximately constant as discussed above and replaced one kinesin by an Eg5(513)-like motor.

The simulations predict that plus-end directed organelles reduce their speed in the presence of Eg5(513) (Fig. 4A); in agreement with our experimental observations (Fig. 3A, 3G). On the other hand, the simulations do not predict any modifications on the speed of minus-end directed organelles (Fig. 4B); in contrast, the experimental data showed that Eg5(513) reduces the speed of the slowest minus-end directed organelles (Fig. 3H, data corresponding to k= 1). Taken together, these results suggest that the simulations do not reproduce the experimental behavior of minus-end directed organelles in the presence of Eg5(513).

The model also predicts a small reduction on the relative population of the slowest plus-end directed organelles (Fig. 4A) which was not observed in the experiments (Fig. 3A, 3G).

This redistribution depends on the relative amount of Eg5(513) to kinesin arbitrarily set in the simulations which may be very different to the relative amount of motors attached to peroxisomes.

Fig. 4D shows that Eg5(513) generated many new anterograde and retrograde mixed-states (i.e. teams that include different types of motors). Retrograde teams containing Eg5(513) presented similar velocities to equivalent teams with kinesins explaining the invariance of retrograde speed distribution. In contrast, anterograde teams slowed down when Eg5(513) replaced kinesin. The speed distributions of Eg5(513)-containing states were also narrower in agreement with the smaller widths observed experimentally in the presence of the deficient motor.

The symmetric tug of war scenario predicts that Eg5(513) reduces the characteristic length of anterograde runs and increases the retrograde lengths (Table 2), in disagreement with the experiments (Table 1).

We also tested an asymmetric tug of war scenario consisting of 4 weak dyneins competing with 2 strong kinesins. To account for dynein team tenacity against opposing

17

loads [72], we considered that the attachment probability of the motor increases when multiple dyneins engage to the microtubule.

Supplemental Fig. 4 shows that this asymmetric model could not qualitatively reproduce the multimode speed distribution of retrograde peroxisomes even after relaxing constrains on the parameter values or increasing the number of motors involved in the tug of war. For example, a model with 12 dyneins and 6 kinesins shifted the whole anterograde and retrograde speed distributions toward higher values (Supplemental Fig. 5).

The asymmetric model predicts that minus-end directed transport mostly relies on pure dynein teams (Supplemental Fig. 4). In contrast, cargoes moving toward the plus end are mainly driven by either a single kinesin or a kinesin-dynein mixed team (Supplemental Fig. 4). Kinesin replacement by Eg5(513) produced similar effects to those observed with the symmetric model: it does not modify the speed distribution of minus-end directed teams but slowed down plus-end directed transport (Supplemental Fig. 4). On the other hand, plus-end directed run lengths decreased in the presence of the deficient motor whereas minus-end directed runs did not significantly change (Supplemental Table 6) as also expected in the symmetric tug of war scenario.

Taken together, the numerical simulations show that neither the symmetric nor the asymmetric scenario predicts the crosstalk between motors in the slowest teams observed in the experiments. The results support a higher level of complexity in the communication between these teams that is not included in simple tug of war models.
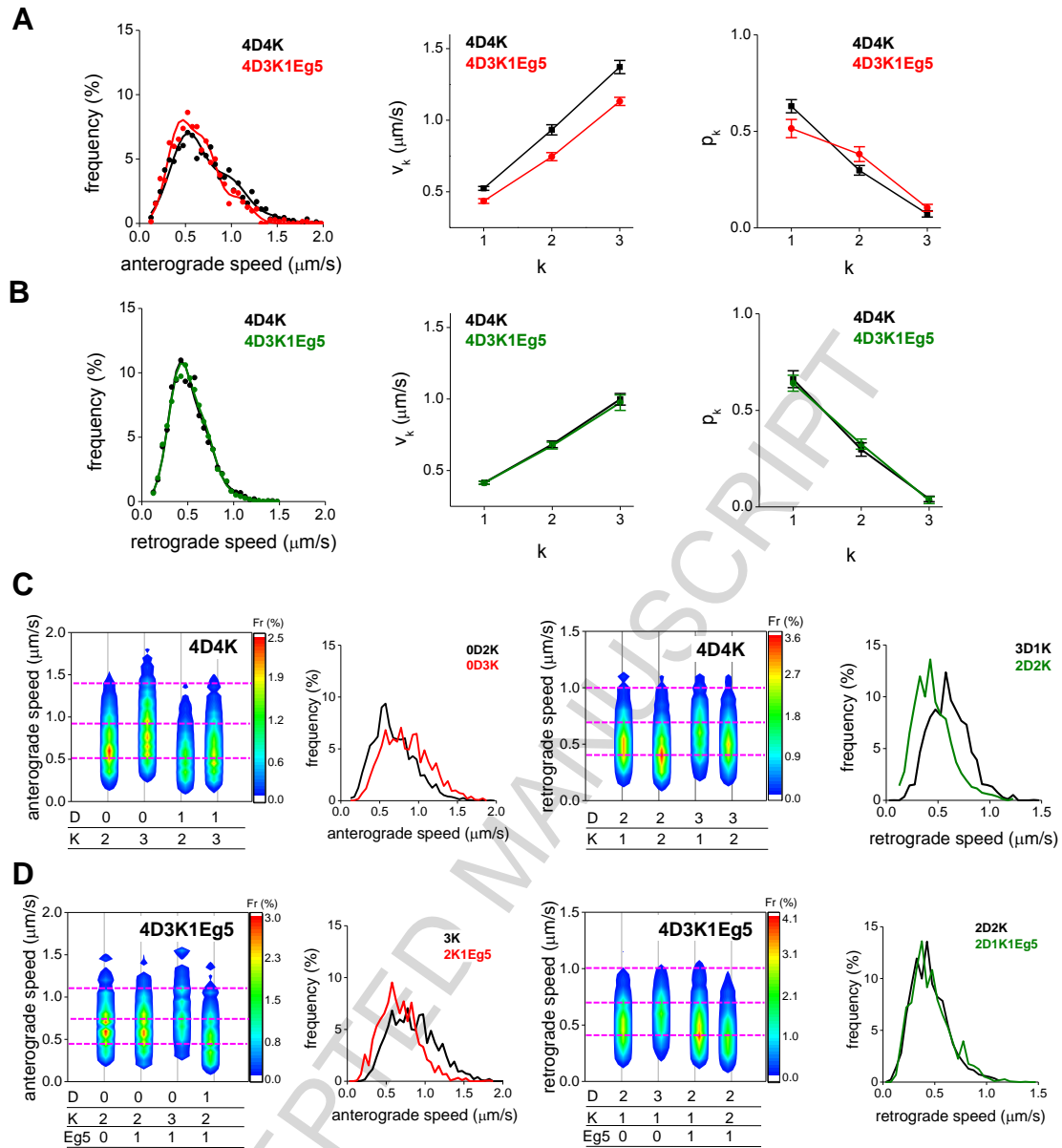
Fig. 4. Numerical simulations of a symmetric tug of war model. The wild type scenario (4D4K) includes 4 dyneins (D) and 4 kinesins (K). One of the kinesins was replaced by an Eg5(513)-like motor (named as Eg5) in the 4D3K1Eg5 scenario. The parameters of the model are detailed in Supplemental Table 1. The simulated trajectories ($N_{trajectories}$=250) were analyzed similarly to the experimental data to obtain the segmental speed distributions of anterograde **(A)** and retrograde **(B)** cargoes. The speed data (circles) was analyzed as described in Section 2.9 considering a mixture of 3 Gaussian functions (Eq. 3, lines) obtaining the v_k and p_k also summarized in Supplemental Tables 4-5. The error bars represent standard errors of each parameter. The motors configurations were obtained for each trajectory segment and correlated with the segmental speeds **(C-D)**. The speed distribution of each motor configuration is represented in pseudocolor, the x-axis details the number of active motors. To facilitate the analysis, the figure only includes the most-probable configurations; the complete data can be found in Supplemental Figs. 6-7. Dotted lines show the characteristic v_k

values obtained in the corresponding scenario. The right panels exemplify the speed distribution of selected configurations.

3.4 The fluidity of peroxisome membrane affects transport

Motors may mechanically communicate with each other through the cargo´s membrane and associated proteins. Nelson et al. [64] demonstrated that the fluidity of the bilayer affects the velocity of myosin teams synthetically anchored to phospholipid vesicles. On the other hand, dyneins cluster into raft-like microdomains on phagosomes improving their performance as a team [73]. These previous works show that the cargo membrane plays a relevant role on the performance of motor teams.

We then asked whether the membrane-mediated mechanical coupling influences the performance of anterograde and retrograde teams during peroxisome transport.

We treated S2 cells expressing Eg5(513)-mCherry-Pex26 with methyl-β-ciclodextrin (MβCD). This drug removes cholesterol from raft and non-raft domains of the plasma membrane and alters the distribution of cholesterol between plasma and intracellular membranes [74].

Since the effects of MβCD on the membranes organization depend on the cell type and specific treatment [74], we used the polarity sensitive probe C-laurdan [28] to evaluate the overall effect of MβCD on S2 membranes (Fig. 5, A-C). Fig. 5D shows that GP values decreased after the treatment suggesting an increase on the fluidity of cellular membranes after the treatment. We identified red-labeled peroxisomes in the images and observed that MβCD also increases their membrane fluidity (Fig. 5D).

To explore whether the membrane fluidity affects peroxisome transport, we tracked these organelles in MβCD-treated S2 cells expressing SKL fused to EGFP. Fig. 5, E-F, shows that anterograde and retrograde organelles presented multimode speed distributions. The characteristic speed of the first mode of these distributions decreased after MβCD treatment suggesting that the fluidity of the membrane influences the mechanical coupling among motors in the slowest teams.

The median run lengths of both anterograde and retrograde organelles did not change after MβCD treatment (Table 1) showing that this drug does not affect the mechanism of deactivation of active teams.
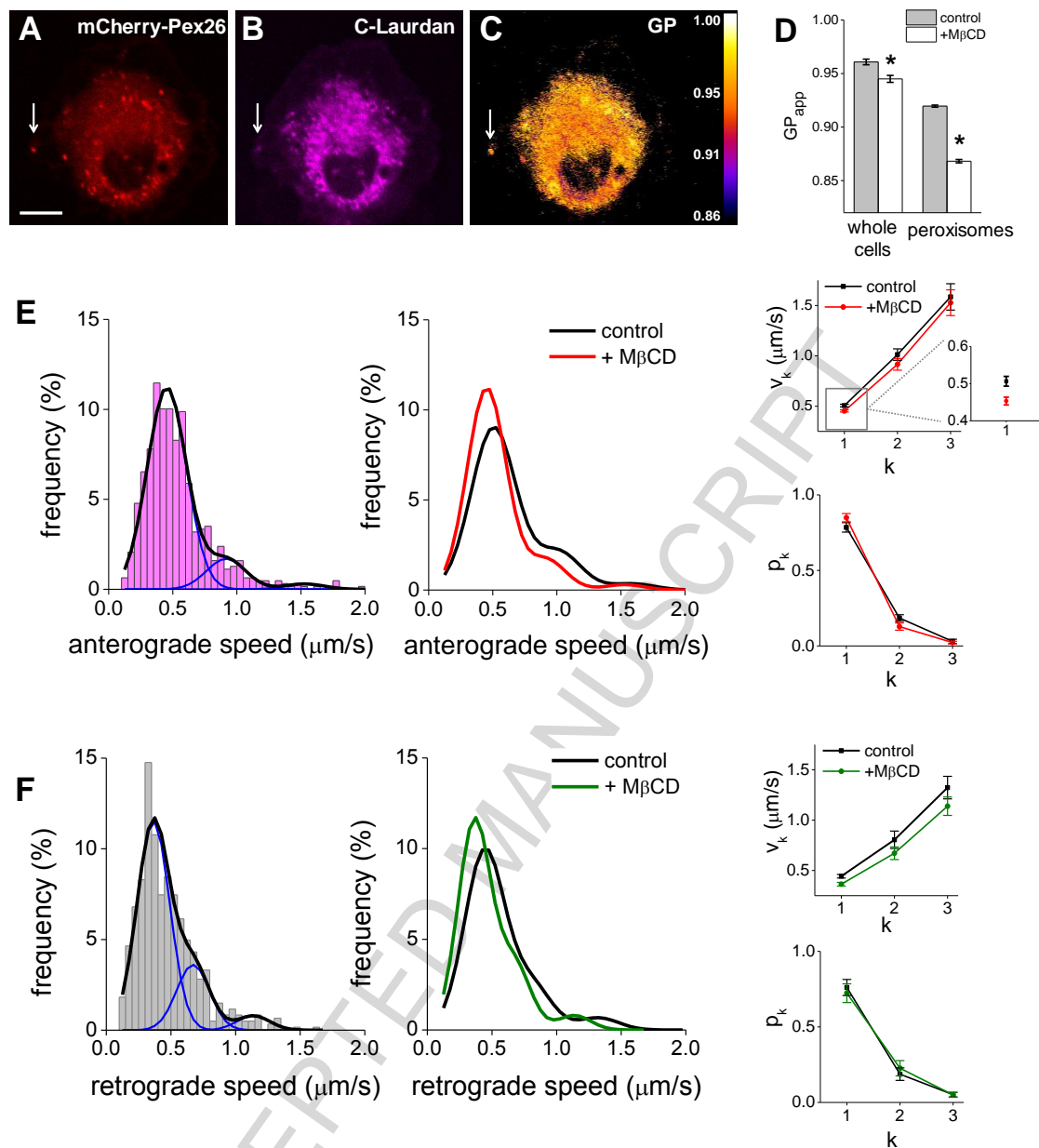
Fig. 5. Influence of peroxisomes membrane fluidity on transport. Representative confocal images of a S2 cell expressing Eg5(513)-mCherry-Pex26 and incubated with the polarity sensitive probe C-Laurdan **(A-B).** The arrow shows a peroxisome. Scale bar: 5 μm. GP images were obtained as described in the text **(C)** and analyzed to recover the mean, apparent GP of either whole cells ($N_{cells}=20$) or isolated peroxisomes ($N_{peroxisomes}=20$) in control and MβCD-treated cells; higher GP values indicate lower membrane fluidities **(D)**. The quantitative analyses of the speeds of anterograde **(E)** and retrograde **(F)** peroxisomes in MβCD treated cells showed that the distribution followed 3-gaussian functions (continuous lines) characterized by the parameters shown in the right panels and Supplemental Tables 2-3. The error bars represents the standard error of each parameter.

4. Discussion

Organelle transport in living cells relies on the action of molecular motors. Dynein, kinesin and myosin activities are modulated by adaptor and regulatory proteins [75] through mechanisms that are generally poorly understood. In addition, microtubules and actin filaments are far from being passive tracks since their intrinsic dynamics, chemical properties and interactions with other proteins affect transport [27, 47, 76, 77]. Moreover, the cytoplasm imposes a drag to motor-cargo complexes that have to find their way through this overcrowded milieu [78]. This complex interplay between different biochemical and physical properties of the intracellular milieu determines that transport cannot be understood by only considering the i*n vitro* properties of the motors.

In this work, we explored how microtubule motors work together during organelle transport scrutinizing the properties of peroxisome trajectories obtained with high spatial and temporal resolutions.

The comparison between experimental and simulated data obtained in simple tug of war scenarios showed that models incorporating strong dynein motors with properties compatible to those measured for the dynein complex with dynactin and Bicaudal [10] recapitulates many but not every property of peroxisome transport. Importantly, the model could explain the multimode speed distributions of retrograde and anterograde peroxisomes also observed for other organelles in living cells [30, 43]. Nevertheless, our observations do not allow ruling out other models with higher levels of regulation. For example, Reis et al. [43] showed that APP vesicle also present velocity distributions with high speed modes that depended on the amount of kinesin-1. The authors suggest that opposed-polarity motors assemble in stable teams and control both, the speed and direction of the vesicles through dynein intermediate chain. This example shows that it might be possible that the relative amount of fast organelles and their speed may result from a combination of a tug of war and unknown regulatory mechanisms.

In addition, we cannot also rule out that longitudinal sliding of microtubules [76] has a minor contribution to the speed distributions. This process may also explain some of the divergences between the experimental distributions and the predictions of the symmetric tug of war model.

In this work, we expressed in the cells plus-end directed motors tagged to peroxisomes; their competition with the endogenous cytoplasmic dynein and kinesin-1 allowed detecting some important features of bidirectional transport along microtubules.

Expression of Pex-targeted KHC576 did not modify retrograde transport (Fig. 3H and Supplemental Table 3) whereas it slightly slowed down plus-end directed organelles (Fig. 3G and Supplemental Table 2) without affecting their run lengths (Table 1). These observations have two relevant implications. First, the number of kinesin motors engaged in active teams seems to be independent on the density of kinesins on the cargo in line with previous works [60]. In addition, we speculate that the performance of kinesin in peroxisome transport seems to be independent on regulatory mechanisms

22

depending on KLC or the C-terminal portion of KHC which is not present in our mutant kinesin motor. The interaction between kinesin light chain and the intermediate chain of dynein [79] was previously proposed to coordinate kinesin and dynein during amyloid precursor protein vesicles transport in neurons [43]. Our observations suggest that this mechanism might not play a determinant role during peroxisome transport.

Peroxisome transport was affected by the slow plus-end directed motor Eg5(513)-mCherry-Pex26. Anterograde peroxisome transport significantly slowed down in the presence of Eg5(513)-mCherry-Pex26 in line with previous gliding assays and numerical simulations showing that Eg5 slows down microtubules carried by kinesin-1 [80]. Unexpectedly, retrograde transport was also perturbed by Eg5(513)-mCherry-Pex26 since both, the speed of the slowest teams and the characteristic run length decreased in the presence of this motor. These results could not be explained with our simple tug of war scenarios and suggest a crosstalk between anterograde and retrograde motors.

In addition, increasing the fluidity of peroxisome membranes with MβCD reduced the speed of slow anterograde and retrograde peroxisomes that are likely undergoing a tug-of-war suggesting that the membrane plays an relevant role on the performance and possibly on the mechanical communication among motors in these slow teams.

The interdependence of opposed-polarity teams has been reported in other *in vivo* transport systems and explained through different mechanisms including the coordination of teams by regulatory proteins, the microtubule tethering model and the mechanical coupling of opposed teams (reviewed in [1]) . Specifically, the second model considers that opposing motor teams remains in weak binding state tethering cargo to the microtubule. In this context, the reason why inhibiting one motor diminishes cargo transport by the opposing motor is that the tethering of the cargo to the microtubule is reduced, and the cargo then tends to dissociate from the microtubule. The last model postulates that motors are predominantly in an inactive state at low load forces and forces generated by opposing motors bound to the same cargo pull the motor out of this inhibited state, freeing it for active motion. Thus, the model proposes that the activation of a motor is regulated by forces generated by the opposed-polarity motors.

Our data could not be explained through microtubule tethering since Eg5(513) should provide the same weak interaction with the track as the endogenous motors and thus should not affect retrograde transport. Slow anterograde and retrograde teams probably communicate mechanically through the membrane and/or other unknown regulatory proteins.

Recently, Reddy et al. [81] showed that an opposed force facilitates the interaction of dynein with LIS1 and NudE/L generating stronger teams. If this were the case during peroxisome transport, a deficient plus-end directed motor and/or partial decoupling of teams through a more-fluid membrane could interfere with this mechanism reducing the speed of the slow retrograde team. We could also hypothesize that the shorter retrograde

23

run lengths observed in the presence of Eg5(513) are explained by an inefficient coupling between opposed teams triggering the release of the cargo from the track. Whereas no molecular mechanism has been proposed for the mechanical activation of kinesin, organelles such as lipid droplets moving toward the plus or minus-ends have shown to preserve some memory on their directionality after brief stalls [82]. This result suggests that some relatively stable and cooperative assembly among motors is required for initiating both, anterograde and retrograde transport.

Acknowledgments

References

[1] W.O. Hancock, Bidirectional cargo transport: moving beyond tug of war, Nat Rev Mol Cell Biol, 15 (2014) 615-628.

[2] M.A. Welte, Bidirectional transport along microtubules, Curr Biol, 14 (2004) R525-537.

[3] N. Hirokawa, Y. Noda, Y. Tanaka, S. Niwa, Kinesin superfamily motor proteins and intracellular transport, Nat Rev Mol Cell Biol, 10 (2009) 682-696.

[4] K.J. De Vos, A.J. Grierson, S. Ackerley, C.C. Miller, Role of axonal transport in neurodegenerative diseases, Annu Rev Neurosci, 31 (2008) 151-173.

[5] E. Chevalier-Larsen, E.L. Holzbaur, Axonal transport and neurodegenerative disease, Biochim Biophys Acta, 1762 (2006) 1094-1108.

[6] L.G. Bilsland, E. Sahai, G. Kelly, M. Golding, L. Greensmith, G. Schiavo, Deficits in axonal transport precede ALS symptoms in vivo, Proc Natl Acad Sci U S A, 107 (2010) 20523-20528.

[7] G.A. Morfini, Y.M. You, S.L. Pollema, A. Kaminska, K. Liu, K. Yoshioka, B. Bjorkblom, E.T. Coffey, C. Bagnato, D. Han, C.F. Huang, G. Banker, G. Pigino, S.T. Brady, Pathogenic huntingtin inhibits fast axonal transport by activating JNK3 and phosphorylating kinesin, Nat Neurosci, 12 (2009) 864-871.

[8] A.L. Strom, J. Gal, P. Shi, E.J. Kasarskis, L.J. Hayward, H. Zhu, Retrograde axonal transport and motor neuron disease, J Neurochem, 106 (2008) 495-505.

[9] E. Perlson, G.B. Jeong, J.L. Ross, R. Dixit, K.E. Wallace, R.G. Kalb, E.L. Holzbaur, A switch in retrograde signaling from survival to stress in rapid-onset neurodegeneration, J Neurosci, 29 (2009) 9903-9917.

[10] V. Belyy, M.A. Schlager, H. Foster, A.E. Reimer, A.P. Carter, A. Yildiz, The mammalian dynein-dynactin complex is a strong opponent to kinesin in a tug-of-war competition, Nat Cell Biol, 18 (2016) 1018-1024.

[11] A. Yildiz, M. Tomishige, R.D. Vale, P.R. Selvin, Kinesin walks hand-over-hand, Science, 303 (2004) 676-678.

[12] R. Mallik, B.C. Carter, S.A. Lex, S.J. King, S.P. Gross, Cytoplasmic dynein functions as a gear in response to load, Nature, 427 (2004) 649-652.

[13] S.L. Reck-Peterson, A. Yildiz, A.P. Carter, A. Gennerich, N. Zhang, R.D. Vale, Single-molecule analysis of dynein processivity and stepping behavior, Cell, 126 (2006) 335-348.

[14] M.J. Muller, S. Klumpp, R. Lipowsky, Tug-of-war as a cooperative mechanism for bidirectional cargo transport by molecular motors, Proc Natl Acad Sci U S A, 105 (2008) 4609-4614.

[15] V. Soppina, A.K. Rai, A.J. Ramaiya, P. Barak, R. Mallik, Tug-of-war between dissimilar teams of microtubule motors regulates transport and fission of endosomes, Proc Natl Acad Sci U S A, 106 (2009) 19381-19386.

[16] R.T. McLaughlin, M.R. Diehl, A.B. Kolomeisky, Collective dynamics of processive cytoskeletal motors, Soft Matter, 12 (2016) 14-21.

[17] T.L. Blasius, D. Cai, G.T. Jih, C.P. Toret, K.J. Verhey, Two binding partners cooperate to activate the molecular motor Kinesin-1, J Cell Biol, 176 (2007) 11-17.

[18] M.M. Fu, E.L. Holzbaur, Integrated regulation of motor-driven organelle transport by scaffolding proteins, Trends Cell Biol, 24 (2014) 564-574.

[19] B.H. Blehm, P.R. Selvin, Single-molecule fluorescence and in vivo optical traps: how multiple dyneins and kinesins interact, Chem Rev, 114 (2014) 3335-3352.

[20] S. Ally, A.G. Larson, K. Barlan, S.E. Rice, V.I. Gelfand, Opposite-polarity motors activate one another to trigger cargo transport in live cells, J Cell Biol, 187 (2009) 1071-1082.

[21] C. Kural, H. Kim, S. Syed, G. Goshima, V.I. Gelfand, P.R. Selvin, Kinesin and dynein move a peroxisome in vivo: a tug-of-war or coordinated movement?, Science, 308 (2005) 1469-1472.

[22] H. Kim, S.C. Ling, G.C. Rogers, C. Kural, P.R. Selvin, S.L. Rogers, V.I. Gelfand, Microtubule binding by dynactin is required for microtubule organization but not cargo transport, J Cell Biol, 176 (2007) 641-651.

[23] S.C. Ling, P.S. Fahrner, W.T. Greenough, V.I. Gelfand, Transport of Drosophila fragile X mental retardation protein-containing ribonucleoprotein granules by kinesin-1 and cytoplasmic dynein, Proc Natl Acad Sci U S A, 101 (2004) 17428-17433.

[24] Y. Aboelkassem, J.A. Bonilla, K.J. McCabe, S.G. Campbell, Contributions of Ca(2+)-Independent Thin Filament Activation to Cardiac Muscle Function, Biophys J, 109 (2015) 2101-2112.

[25] K.J. Verhey, D.L. Lizotte, T. Abramson, L. Barenboim, B.J. Schnapp, T.A. Rapoport, Light chain-dependent regulation of Kinesin's interaction with microtubules, J Cell Biol, 143 (1998) 1053-1066.

[26] D.S. Friedman, R.D. Vale, Single-molecule analysis of kinesin motility reveals regulation by the cargo-binding tail domain, Nat Cell Biol, 1 (1999) 293-297.

[27] D. Cai, D.P. McEwen, J.R. Martens, E. Meyhofer, K.J. Verhey, Single molecule imaging reveals differences in microtubule track selection between Kinesin motors, PLoS Biol, 7 (2009) e1000216.

[28] M.M. Dodes Traian, F.L. Gonzalez Flecha, V. Levi, Imaging lipid lateral organization in membranes with C-laurdan in a confocal microscope, J Lipid Res, 53 (2012) 609-616.

[29] H.M. Kim, H.J. Choo, S.Y. Jung, Y.G. Ko, W.H. Park, S.J. Jeon, C.H. Kim, T. Joo, B.R. Cho, A two-photon fluorescent probe for lipid raft imaging: C-laurdan, Chembiochem, 8 (2007) 553-559.

[30] V. Levi, A.S. Serpinskaya, E. Gratton, V. Gelfand, Organelle transport along microtubules in Xenopus melanophores: evidence for cooperation between multiple motors, Biophys J, 90 (2006) 318-327.

[31] A. Kunwar, A. Mogilner, Robust transport by multiple motors with nonlinear force-velocity relations and stochastic load sharing, Phys Biol, 7 (2010) 16012.

[32] M.J. Muller, S. Klumpp, R. Lipowsky, Bidirectional transport by molecular motors: enhanced processivity and response to external forces, Biophys J, 98 (2010) 2610-2618.

[33] S. Bouzat, V. Levi, L. Bruno, Transport properties of melanosomes along microtubules interpreted by a tug-of-war model with loose mechanical coupling, PLoS One, 7 (2012) e43599.

[34] M.C. De Rossi, M.E. De Rossi, M. Sued, D. Rodriguez, L. Bruno, V. Levi, Asymmetries in kinesin-2 and cytoplasmic dynein contributions to melanosome transport, FEBS Lett, 589 (2015) 2763-2768.

[35] M.T. Valentine, P.M. Fordyce, T.C. Krzysiak, S.P. Gilbert, S.M. Block, Individual dimers of the mitotic kinesin motor Eg5 step processively and support substantial loads in vitro, Nat Cell Biol, 8 (2006) 470-476.

[36] L. Wasserman, All of statistics: A concise course in statistical inference, in, Springer-Verlag. New York., 2010.

[37] W.H. Render RA, Mixture Densities, Maximum Likelihood and the EM Algorithm, in, vol. 26, SIAM Review, 1984.

[38] G. Schwarz, Estimating the dimension of a model, The annals of statistics, 62 (1978) 461-464.

[39] L. Wasserman, All of statistics: A concise course in statistical inference, Springer-Verlag, New York, 2010.

[40] F.D. Corder GW, Nonparametric Statistics: A Step-by-Step Approach, 2nd Edition, in, John Wiley & Sons, Inc., 2014.

[41] C. Pallavicini, V. Levi, D.E. Wetzler, J.F. Angiolini, L. Bensenor, M.A. Desposito, L. Bruno, Lateral Motion and Bending of Microtubules Studied with a New Single-Filament Tracking Routine in Living Cells, Biophys J, 106 (2014) 2625-2635.

[42] S.E. Encalada, L.S. Goldstein, Biophysical challenges to axonal transport: motor-cargo deficiencies and neurodegeneration, Annu Rev Biophys, 43 (2014) 141-169.

[43] G.F. Reis, G. Yang, L. Szpankowski, C. Weaver, S.B. Shah, J.T. Robinson, T.S. Hays, G. Danuser, L.S. Goldstein, Molecular motor function in axonal transport in vivo probed by genetic and computational analysis in Drosophila, Mol Biol Cell, 23 (2012) 1700-1714.

[44] S.E. Encalada, L. Szpankowski, C.H. Xia, L.S. Goldstein, Stable kinesin and dynein assemblies drive the axonal transport of mammalian prion protein vesicles, Cell, 144 (2011) 551-565.

[45] J. Xu, Z. Shu, S.J. King, S.P. Gross, Tuning multiple motor travel via single motor velocity, Traffic, 13 (2012) 1198-1205.

[46] R. Mallik, D. Petrov, S.A. Lex, S.J. King, S.P. Gross, Building complexity: an in vitro study of cytoplasmic dynein with in vivo implications, Curr Biol, 15 (2005) 2075-2085.

[47] M. Vershinin, B.C. Carter, D.S. Razafsky, S.J. King, S.P. Gross, Multiple-motor based transport and its regulation by Tau, Proc Natl Acad Sci U S A, 104 (2007) 87-92.

[48] R.J. McKenney, W. Huynh, M.E. Tanenbaum, G. Bhabha, R.D. Vale, Activation of cytoplasmic dynein motility by dynactin-cargo adapter complexes, Science, 345 (2014) 337-341.

[49] A.S. Kashina, R.J. Baskin, D.G. Cole, K.P. Wedaman, W.M. Saxton, J.M. Scholey, A bipolar kinesin, Nature, 379 (1996) 270-272.

[50] L.C. Kapitein, E.J. Peterman, B.H. Kwok, J.H. Kim, T.M. Kapoor, C.F. Schmidt, The bipolar mitotic kinesin Eg5 moves on both microtubules that it crosslinks, Nature, 435 (2005) 114-118.

[51] T.C. Krzysiak, T. Wendt, L.R. Sproul, P. Tittmann, H. Gross, S.P. Gilbert, A. Hoenger, A structural model for monastrol inhibition of dimeric kinesin Eg5, Embo J, 25 (2006) 2263-2273.

[52] M.T. Valentine, S.P. Gilbert, To step or not to step? How biochemistry and mechanics influence processivity in Kinesin and Eg5, Curr Opin Cell Biol, 19 (2007) 75-81.

[53] G.Y. Chen, K.J. Mickolajczyk, W.O. Hancock, The Kinesin-5 Chemomechanical Cycle Is Dominated by a Two-heads-bound State, J Biol Chem, 291 (2016) 20283-20294.

[54] D.D. Hackney, Highly processive microtubule-stimulated ATP hydrolysis by dimeric kinesin head domains, Nature, 377 (1995) 448-450.

[55] O. Campas, C. Leduc, P. Bassereau, J. Casademunt, J.F. Joanny, J. Prost, Coordination of Kinesin motors pulling on fluid membranes, Biophys J, 94 (2008) 5009-5017.

[56] D. Cai, K.J. Verhey, E. Meyhofer, Tracking single Kinesin molecules in the cytoplasm of mammalian cells, Biophys J, 92 (2007) 4137-4144.

[57] D. Cai, A.D. Hoppe, J.A. Swanson, K.J. Verhey, Kinesin-1 structural organization and conformational changes revealed by FRET stoichiometry in live cells, J Cell Biol, 176 (2007) 51-63.

[58] P. Bieling, I.A. Telley, J. Piehler, T. Surrey, Processive kinesins require loose mechanical coupling for efficient collective motility, EMBO Rep, 9 (2008) 1121-1127.

[59] K.S. Müller M. J. I. , Lipowsky R., Motility States of Molecular Motors Engaged in a Stochastic Tug-of-War in, vol. 133,1059, Journal of Statistical Physics, 2008.

[60] A.K. Efremov, A. Radhakrishnan, D.S. Tsao, C.S. Bookwalter, K.M. Trybus, M.R. Diehl, Delineating cooperative responses of processive motors in living cells, Proc Natl Acad Sci U S A, 111 (2014) E334-343.

[61] A.K. Rai, A. Rai, A.J. Ramaiya, R. Jha, R. Mallik, Molecular adaptations allow dynein to generate large collective forces inside cells, Cell, 152 (2013) 172-182.

[62] R.J. McKenney, M. Vershinin, A. Kunwar, R.B. Vallee, S.P. Gross, LIS1 and NudE induce a persistent dynein force-producing state, Cell, 141 (2010) 304-314.

[63] J.M. Sanderson, Resolving the kinetics of lipid, protein and peptide diffusion in membranes, Mol Membr Biol, 29 (2012) 118-143.

[64] S.R. Nelson, K.M. Trybus, D.M. Warshaw, Motor coupling through lipid membranes enhances transport velocities for ensembles of myosin Va, Proc Natl Acad Sci U S A, 111 (2014) E3986-3995.

[65] R.P. Erickson, Z. Jia, S.P. Gross, C.C. Yu, How molecular motors are arranged on a cargo is important for vesicular transport, PLoS Comput Biol, 7 (2011) e1002032.

[66] A. Kunwar, M. Vershinin, J. Xu, S.P. Gross, Stepping, strain gating, and an unexpected force-velocity curve for multiple-motor-based transport, Curr Biol, 18 (2008) 1173-1183.

[67] C.M. Coppin, D.W. Pierce, L. Hsu, R.D. Vale, The load dependence of kinesin's mechanical cycle, Proc Natl Acad Sci U S A, 94 (1997) 8539-8544.

[68] L. Bruno, M. Salierno, D.E. Wetzler, M.A. Desposito, V. Levi, Mechanical properties of organelles driven by microtubule-dependent molecular motors in living cells, PLoS One, 6 (2011) e18332.

[69] J. Beeg, S. Klumpp, R. Dimova, R.S. Gracia, E. Unger, R. Lipowsky, Transport of beads by several kinesin motors, Biophys J, 94 (2008) 532-541.

[70] M.J. Schnitzer, K. Visscher, S.M. Block, Force production by single kinesin motors, Nat Cell Biol, 2 (2000) 718-723.

[71] C. Leduc, O. Campas, K.B. Zeldovich, A. Roux, P. Jolimaitre, L. Bourel-Bonnet, B. Goud, J.F. Joanny, P. Bassereau, J. Prost, Cooperative extraction of membrane nanotubes by molecular motors, Proc Natl Acad Sci U S A, 101 (2004) 17096-17101.

[72] R. Mallik, A.K. Rai, P. Barak, A. Rai, A. Kunwar, Teamwork in microtubule motors, Trends Cell Biol, 23 (2013) 575-582.

[73] A. Rai, D. Pathak, S. Thakur, S. Singh, A.K. Dubey, R. Mallik, Dynein clusters into lipid microdomains on phagosomes to drive rapid transport toward lysosomes, Cell, 164 (2016) 722-734.

[74] R. Zidovetzki, I. Levitan, Use of cyclodextrins to manipulate plasma membrane cholesterol content: evidence, misconceptions and control strategies, Biochim Biophys Acta, 1768 (2007) 1311-1324.

[75] A. Akhmanova, J.A. Hammer, 3rd, Linking molecular motors to membrane cargo, Curr Opin Cell Biol, 22 (2010) 479-487.

[76] I.M. Kulic, A.E.X. Brown, H. Kim, C. Kural, B. Blehm, P.R. Selvin, P.C. Nelson, V. Gelfand, The role of microtubule movement in bidirectional organelle transport, Proc Natl Acad Sci U S A, 105 (2008) 10011-10016.

[77] R. Dixit, J.L. Ross, Y.E. Goldman, E.L. Holzbaur, Differential regulation of dynein and kinesin motor proteins by tau, Science, 319 (2008) 1086-1089.

[78] B. Wang, J. Kuo, S. Granick, Bursts of active transport in living cells, Phys Rev Lett, 111 (2013) 208102.

[79] L.A. Ligon, M. Tokito, J.M. Finklestein, F.E. Grossman, E.L. Holzbaur, A direct interaction between cytoplasmic dynein and kinesin I may coordinate motor activity, J Biol Chem, 279 (2004) 19201-19208.

[80] G. Arpag, S. Shastry, W.O. Hancock, E. Tuzel, Transport by populations of fast and slow kinesins uncovers novel family-dependent motor characteristics important for in vivo function, Biophys J, 107 (2014) 1896-1904.

[81] B.J. Reddy, M. Mattson, C.L. Wynne, O. Vadpey, A. Durra, D. Chapman, R.B. Vallee, S.P. Gross, Load-induced enhancement of Dynein force production by LIS1-NudE in vivo and in vitro, Nat Commun, 7 (2016) 12259.

[82] C. Leidel, R.A. Longoria, F.M. Gutierrez, G.T. Shubeita, Measuring molecular motor forces in vivo: implications for tug-of-war models of bidirectional transport, Biophys J, 103 (2012) 492-500.

TABLES

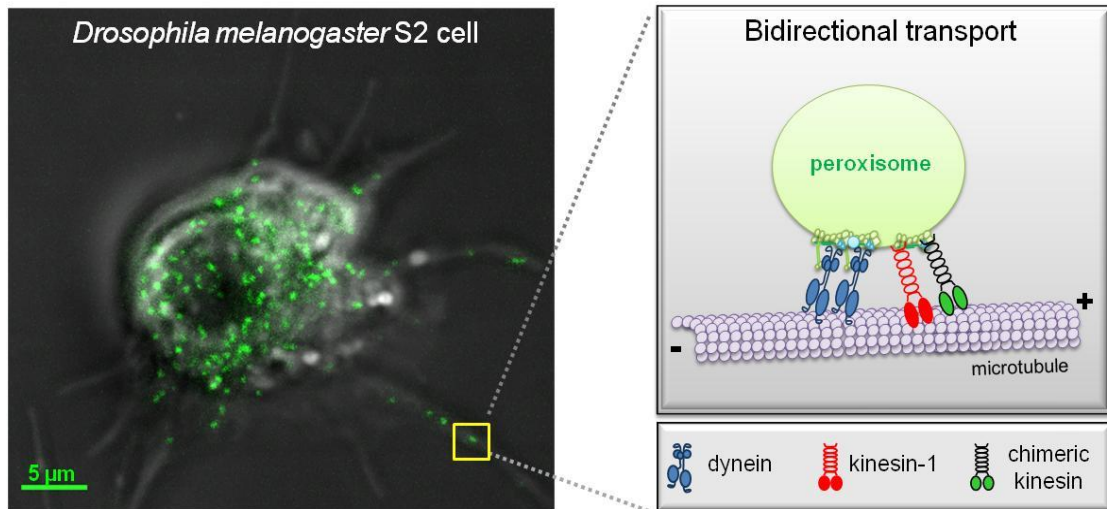| condition	retrograde runs (nm)	anterograde runs (nm)
wild type	1064 ± 70	991 ± 110
+ Eg5(513)	822 ± 84 (*)	833 ± 50 (*)
+ KHC 576	1087 ± 77	1058 ± 103
+ MβCD	1083 ± 96	1057 ± 109

Table 1. Anterograde an retrograde peroxisomes run lengths. The data is expressed as median ± standard error. Asterisks denote significant differences between values (p-value<0.05).

simulation	retrograde runs (nm)	anterograde runs (nm)
4D-4K	684 ± 19	885 ± 27
4D-3K-1Eg5	736 ± 11 (*)	727 ± 22 (*)

Table 2. Run lengths obtained in the symmetric tug of war simulations. Eg5 stands for Eg5(513). The data is expressed as median ± standard error. Asterisks denote significant differences between values (p-value<0.05).

Graphical Abstract

Highlights

- We studied the properties of peroxisomes transport driven by kinesin-1 and dynein
- Speeds of anterograde and retrograde organelles were statistically analyzed
- Expression of slow chimeric plus-end directed motor influenced peroxisome transport
- The fluidity of organelles membrane modified the speed of motors teams
- Opposed-polarity motors mechanically communicate with each other